The Impact of Chaotic Advection on the Microstructure of Polymer-Modified Bitumen

Maria P. Bracciale, Alessandra Broggi, Stefano Cerbelli, Marco Formisano, Maria L. Santarelli, and Marco Scarsella
Dipartimento di Ingegneria Chimica Materiali Ambiente, Sapienza Università di Roma Via Eudossiana 18, 00184 Rome, Italy

Assunta Marrocchi
Dipartimento di Chimica, Università di Perugia, Via Elce di Sotto 8, 06123, Perugia, Italy

DOI 10.1002/aic.14361
Published online January 29, 2014 in Wiley Online Library (wileyonlinelibrary.com)

Owing to the high viscosity of the materials involved, mixing is often a critical step when processing polymer-modified bitumen (PMB), directly influencing the microstructure and the stability of final products. We provide experimental evidence suggesting that laminar chaotic advection may prove a valuable strategy for obtaining a homogeneous and finely interdispersed polymer-bitumen mixture in affordable time. As a case study, we investigate the mixing performance of a lab-scale flat-bottomed cylindrical vessel stirred by a radial impeller, either located symmetrically or eccentrically with respect to the vessel axis. The same geometries with a flat-disk impeller are also considered for comparison. The Mix-Norm is used in combination with image analysis as an objective measure of mixing performance. Results of mixing performance are independently validated by rheological tests. The experiments pinpoint kinematic chaos as the fundamental transport mechanism enhancing both the dispersion process and the microstructural quality of the resulting PMBs mixture. © 2014 American Institute of Chemical Engineers *AIChE J*, 60: 1870–1879, 2014
Keywords: chaotic advection, polymer-modified bitumen, mix-norm, mixing time

Introduction

The use of polymer-modified Bitumens (PMBs) has been gaining increasing importance over the past decades in both road building and maintenance, for key products, such as waterproofing sheets/binders for surface dressing, mastic, and porous asphalt.[1] There exists a wide variety of polymers potentially appropriate for such applications, among which Stirene-Butadiene-Styrene (SBS) copolymers and ethylene-vinyl-acetate are most frequently used. The PMBs are very complex systems where the coexistence of two fluids in some degree immiscible (i.e., polymer and bitumen) may yield unstable phase behavior. The system complexity is related to the colloidal structure of bitumen as well as PMB,[2–4] which is ultimately dependent on the chemical composition of the bitumen. Specifically, the proportion of maltenes (i.e., resins and saturated and aromatic oils) and asphaltenes plays a key role in determining the compatibility with a polymer, that is, the extent of segregation between the bitumen and the polymer. In pure bitumen, maltenes (especially polar aromatics) disperse asphaltene particles perfectly. In parallel, polymers act as solid/semisolid particles in modified bitumen so, like asphaltenes, they need a suitable dispersion agent to reach a complete homogeneity. Whereas maltenes disperse polymer particles, thus potentially leading to a unique phase,[5] asphaltenes are not absorbed by these latter. However, in the PMBs, the amount of maltenes may be not sufficient for both asphaltene and polymer particles. In this case, a three component system comprising a phase rich in asphaltenes, a polymer rich phase, and a mixed phase would be obtained. It has been observed[6,7] that the mixed phase may be considered as thermodynamically stable. On the opposite, the remaining two phases are unstable and tend to separate from each other, owing to particle coalescence and gravity. For instance, the polybutadiene segments in the SBS copolymer are miscible in the bitumen, whereas the polystyrene segments are not miscible and phase separation may result.[8] By reason of the above, a major concern when using bitumen/polymer mixtures is their lack of stability, especially when prolonged permanence at high temperatures is involved. The tendency to phase separation appears an important limitation for practical use of PMBs, especially as regards road applications, where the percentage of polymer in the bitumen is low and the separation facilitated. Conversely, it has been observed how the microstructure of the multiphase mixture may have an important influence on the kinetics of phase separation in that Brownian motion of the polymer dispersed particles can slow down sensitively the approach to the gravity-driven multiphase equilibrium.[9] Given that the microstructure of the multiphase system is ultimately dependent on the transport processes occurring when the molten polymer and bitumen are blended with one another, this observation identifies

Correspondence concerning this article should be addressed to M.L. Santarelli at marialaura.santarelli@uniroma1.it

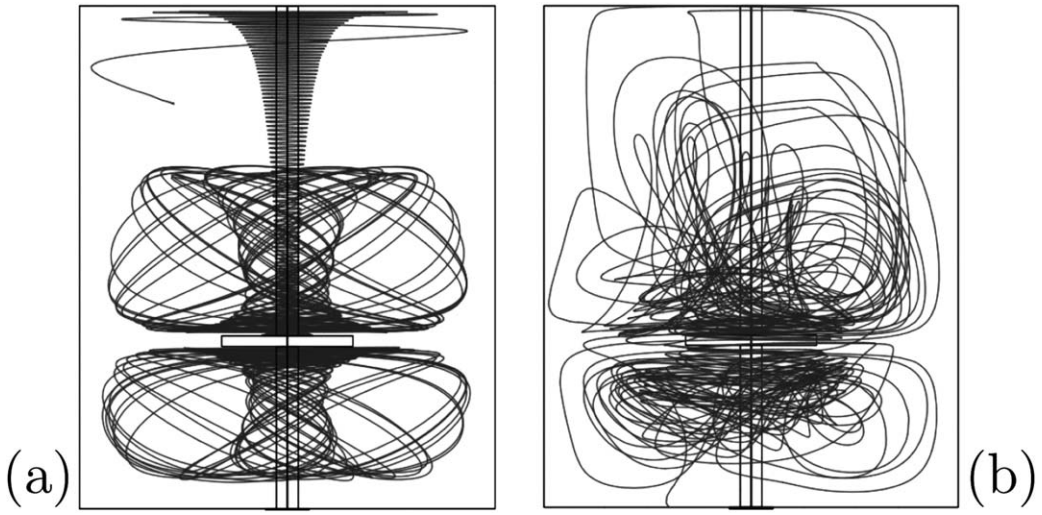

Figure 1. Kinematic trajectories in a Navier-Stokes flow ($Re = 50$) generated by a flat disk rotating inside a cylindrical vessel in the case of (a) symmetric configuration and (b) eccentric geometry.

For visualization purposes, the view angle of panel (b) is parallel to the unique plane of symmetry of the system.

the mixing stage as the key issue for controlling product quality. One notes that, because of the large values of viscosity of the mixture, turbulent fluctuations of the molten material are obtained only at the cost of feeding high energy input to the mixing system,[10] which in turn imposes severe mechanical constraints to the equipment.[11]

Besides, in the last decades, an alternative approach to mixing, referred to as chaotic advection, has been developed, which is not based upon turbulent transport and that can, therefore, be applied effectively even in laminar flows (see, e.g., Refs. 12,13 and therein cited references for an updated account of the state of the art of laminar chaos theory). The scope of this article is to explore the potential of mixing strategies based on chaotic advection for controlling the microstructure of PMB. In the next section, a concise background on the theory—strictly limited to the issues that are relevant to the present work—is reported.

Mixing enhancement by chaotic advection

As discussed above, the practical difficulty of obtaining turbulent flow conditions when blending molten polymer and bitumen makes the optimal design of the mixing stage a challenging task in the layout of the industrial production process. From the standpoint of transport dynamics, turbulent fluctuations are sought in view of their effective dispersion mechanism, which ultimately hinges on the creation, displacement, deformation, and annihilation of turbulent eddies that are continuously regenerated within the moving fluid.

Nearly 30 years ago, Aref[14] showed how the basic template that causes enhanced dispersion in turbulent flows—notably recursive stretching *and* folding of material lines and surfaces—could be "artificially" reproduced even in simple, if purposely designed, laminar flows. The main novelty introduced by Aref's work was that mixing efficiency should not be judged based on the bare structure of the velocity field but rather by the kinematic features of the partially mixed structures that are created by the flow. This approach unveiled a surprisingly rich dynamics of the mixing process even in remarkably simple flows, thus establishing a strong connection between chaotic behavior of fluid element trajectories and mixing efficiency.[15] Based on these concepts, the possibility of obtaining efficient mixing in stirred tanks processing highly viscous fluid was extensively investigated in a series of works, which identified symmetry-breaking of the equipment geometry as one of the most effective routes to massive chaotic behavior.[16–20] For instance, in contrast to what a naive, intuition-based approach would suggest, it was showed that whenever laminar regime prevails, an eccentric placement of the stirrer in a cylindrical vessel could shrink down the mixing time by orders of magnitude when compared to the standard symmetric configuration.

To provide an illustrative example in Figure 1, we show the structure of few trajectories of a passive tracer for the case of a flat bottomed cylindrical vessel stirred by a flat disk for a Newtonian fluid in the laminar regime ($Re = \rho\omega RD/\mu = 50$, ρ, and μ being the fluid density and dynamic viscosity, ω, and R being the disk round per minute (RPM) and radius, and D being the vessel diameter, respectively) in the case of symmetric (Figure 1a), and eccentrically (Figure 1b) positioned impeller. The trajectories were obtained by integrating the advection equation $\dot{\mathbf{x}} = \mathbf{v}(\mathbf{x})$ with a variable step-size integrator, $\mathbf{v}$ being the numerical solution of the steady Navier-Stokes problem obtained through a commercial software (COMSOL (registered trademark of commercial CFD software) multiphysics) using order half million tetrahedral elements. As can be noted, in the first case two trajectories originated at different initial positions are confined onto two kinematically invariant toroidal surfaces. The toroidal regions enclosed by these surfaces are kinematically invariant subsets of the flow domain. It follows that material enclosed in these regions can leave the invariant volume only by diffusive transport. Note that this type of kinematic structures have been observed even in vessels stirred by radial impellers operating in the laminar regime, thus implying that the time-periodic perturbations induced by the impeller blades are not sufficient to ensure the breakup of these invariant regions. In contrast, the flow associated with the eccentric geometry is such that trajectories originated at (almost) any point of the mixing space wander endlessly through the flow domain (Figure 1b shows an example of a typical trajectory). In single-phase Navier-Stokes flows, this erratic behavior has been widely recognized as the fingerprint of chaotic stirring and therefore, of efficient mixing.

Table 1. Formulation and Physical Properties of the SBS Copolymer

Molecular structure	Radial
Styrene content	30% by wt
Butadiene content	70% by wt
Oil content	N/A
Antioxidant	Non staining
Specific gravity	0.94 g / cc (ASTM D 792)
Tensile strength	18 MPa (ASTM D 412)
300% modulus	2.5 MPa (ASTM D 412)
Elongation at break	700% (ASTM D 412)
Brookfield viscosity	20 Pa s
Physical form	White pellets

Note that the computational results of Figure 1 do not strictly allow to draw any conclusion as regards the mixing performance of the analyzed geometries in the presence of polymer-bitumen mixtures, since —(1) the molten blend needs not to behave as a Newtonian Fluid (see, e.g., Ref.[21] for an analysis laminar chaotic transport in Newtonian vs. non-Newtonian fluids) (2) the processed material is really a multiphase mixture, an occurrence that makes the numerical computation of the flow field and mixing dynamics a very difficult task.

Conversely, it has been experimentally showed and theoretically justified that the recursive stretching and folding caused by chaotic advection may profoundly enhance both the spatial dispersion and the uniformity of drop-size distribution of unmiscible phases undergoing stirring.[22,23] Next, we use the rationale gathered from the above example and the results of the cited literature as a guidance for designing tailored experiments seeking first evidence of chaos-enhanced polymer dispersion in PMBs.

Materials and Methods

Tested materials

The modified bitumen was obtained from straight run (**SR**) bitumen 70/100 (Softening point 45°C) by the addition of SBS copolymer, whose characteristics are reported in Table 1.

Sample preparation

Polymer-modified bitumen samples were prepared by mixing a SBS copolymer with a preheated (140°C) base bitumen at a polymer content of 4% wt. The modified bitumen was prepared in a cylindrical vessel ($D=10\text{cm}, H=10\text{cm}$) which was kept at constant temperature $T=160$°C. In all of the experimental runs, the RPM of the impeller was fixed so as to obtain a value $Re = 10$ for the Reynolds number. Two different impellers were used as stirrers, that is, a Rushton turbine ($D=4\text{cm}$), and a disk impeller ($D=5\text{cm}, H=1.5\text{cm}$). Note that the qualitative features of the low Reynolds flow are altogether different in the two cases. The bladed impeller generates a time-periodic flow whose frequency is dictated by its number of blades and by the RPM, whereas the disk stirrer yields a steady flow, even in the eccentric configuration. In point of fact, experiments with the disk impeller were performed to rule out the effect of time-periodic velocity fluctuations (that might have a significant impact of the rheological behavior of the PMB in view of its viscoelastic features) and single out the influence of the kinematic backbone governing the dispersion process. Both symmetric and eccentric configurations were considered for the two types of impeller, with an eccentricity $E=e/R=0.42$ (e being the offset of the shaft with respect to the vessel axis, and R being the internal vessel radius), which is the same value as that used in the simulation of Figure 1. Samples of the PMB were drawn at the center of the surface.

Assessment of SBS-modified bitumen microstructure

The assessment of microstructural properties of SBS-modified bitumen samples was performed with a Nikon Optiphot stereomicroscope. Photomicrographs with 100× magnification were taken at room temperature. Sampling was repeated every 60 min, in the first 3 h, and every 30 min afterwards, until no further changes in the PMB microstructure and a homogeneous mixture of polymers in bitumen matrix was observed. The recorded photographs of the different samples were processed for image analysis using ImagJ software (v. 1.47). A square target area with edge corresponding to physical dimension of 0.85 mm was identified at the center of the image to avoid creep effects occurring at the boundary between the drop sample and the microscope slide.

Figure 2a provides an example of one such image. Starting from the image corresponding to this interrogation area, further processing was implemented to identify the polymer–rich phase and the bitumen–rich phase as follows. First, the image was converted to gray scale using $2^8=256$ gray levels, and its Fourier harmonic content computed (see Figure 2b). Note that whenever some degree of segregation is detectable, the harmonic content typically displays a bimodal distribution (See Figure 2d). Thus, a threshold level can be fixed at the relative minimum of the distribution, and black and white colors can be assigned to identify the two phases (Figure 2c). A threshold sensitivity analysis conducted over few test pictures allowed us to conclude that this approach is robust for the case at hand (not shown for brevity). The image so obtained constitutes the basis for the assessment of mixing quality, which was grounded on the concept of Mix-Norm introduced in Ref. 24 The Mix-Norm measures the extent of "mixedness" at various scales associated with a positive field of scalar intensities say $f(\mathbf{x},t)$ (which, in the present case, is set to take values "0" and "1" for the two phases based on the b/w image), where $\mathbf{x}$ is a generic point of the domain. To explain the physical significance of the Mix-Norm, consider a stirring process occurring in a closed impermeable square domain, and let $a_{\mathbf{k}}(t)$ be the Fourier coefficients of the scalar field at a given time t associated with its expansion in complex Fourier series with basis functions $f_{\mathbf{k}}(\mathbf{x})=\exp(i2\pi\mathbf{k}\cdot\mathbf{x})$, $\mathbf{k}$ being a two-dimensional vector of positive or negative integers. In this expansion, it is assumed that $f(\mathbf{x},t)$ possesses zero average over Ω, a condition that can be obtained by subtracting to the initial field its average value $\int_\Omega f(\mathbf{x},t)d\mathbf{x}/\int_\Omega d\mathbf{x}$. The Mix-Norm ϕ is defined by

$$\phi^2=\sum\nolimits_{\mathbf{k}}\lambda_{\mathbf{k}}\ |a_{\mathbf{k}}|^2 \tag{1}$$

where $1/\lambda_{\mathbf{k}}=\sqrt{1+2\pi||\mathbf{k}||^2}$. Because the $\lambda_{\mathbf{k}}$ vanish as $||\mathbf{k}||\to\infty$, segregated areas of smaller and smaller size (i.e., of high frequency energy content) contribute less and less to the value of ϕ. Therefore, a segregated mixture undergoing efficient stirring is characterized by a decreasing value of the Mix-Norm in that large-sized segregated regions are

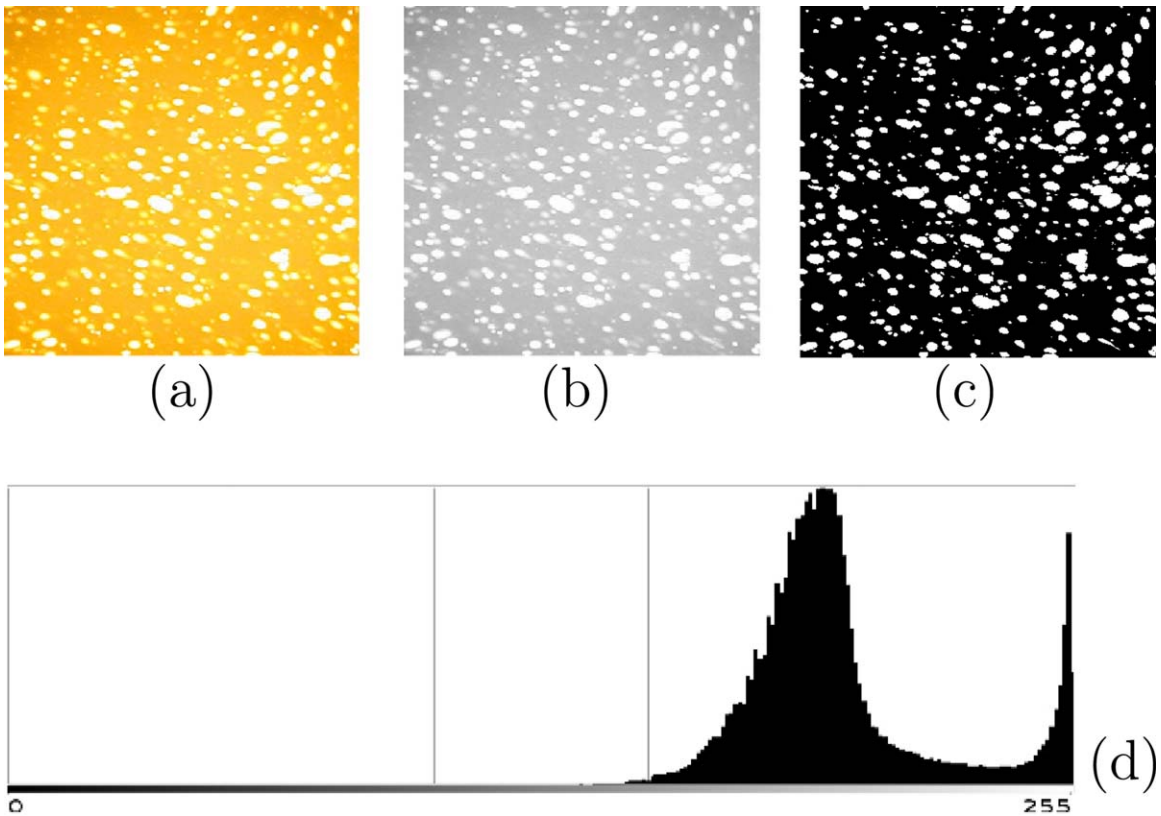

Figure 2. Image processing of the samples (see main text for details).

[Color figure can be viewed in the online issue, which is available at wileyonlinelibrary.com.]

progressively annihilated by the mixing process. Ideally, a perfectly mixed material is characterized by $\phi=0$.

One observes that the Mix-Norm assessment of the degree of mixing cannot be implemented directly in our case, since the samples do not represent a closed system and therefore, the total surface extent of the two phases is not constant and may vary significantly from one sample to another. For this reason, we define a surface index (*SI*) accounting for the total area fraction covered by the polymer–rich phase within the interrogation area, and use it for defining a normalized mixing index (*MI*), given by

$$MI=\phi/SI \tag{2}$$

Note that whenever perfectly mixed conditions*[1] are reached, the *SI* defined above is expected to saturate toward a constant value which is independent of the location of the probe region and that is ultimately dependent only upon the overall relative fraction between the two phases in the entire mixing vessel. The characteristic time needed to reach this saturation value can be envisioned as a mixing time for the system at hand, in accordance to typical approaches to mixing assessment in single-phase flows, be them laminar,[25] or turbulent.[26]

Besides, the *MI* in Eq. 2 yields a weighted average of the residual size of polymer islands as they evolve along with the stirring process, and is, therefore, a measure of the local microstructural properties of the multiphase mixture at any given stage of the polymer dispersion process.

[1]Unlike the case of single-phase systems, these conditions do not define an equilibrium state in that they depend on the presence of continuous stirring is the system.

Rheological measurements

Dynamic rheological tests were performed with a Rheometrics RDA II controlled strain rheometer, using a parallel plate geometry. Frequency sweep runs were applied over the range from 0.1 to 100rad/s under isothermal conditions with 10°C increments. The temperature range scanned was from 0° to 30°C. Eight-millimeter diameter plates with testing gap of 3.0 mm were used. To ensure that frequency sweep tests were being performed within the linear viscoelasticity range of the materials, strain percentage was chosen for each temperature based on strain sweep tests. In dynamic mechanical analysis, the peak stress, the peak strain, and the phase relationship between stress and strain are measured. All of the rheological parameters are determined from these data. The ratio of the peak stress to peak strain is the absolute value of the modulus, referred to as the complex shear modulus $G^*=$ peak stress/peak strain. The elastic in-phase component of G^*, called the shear storage modulus G', and the viscous out-of-phase component of G^*, referred to as G'', are defined as $G'=G^*\cos\delta$ and $G''=G^*\sin\delta$, where δ is the phase angle between the applied maximum strain and the maximum stress. The tangent of the phase angle, $\tan\delta=G''/G'$, yields the ratio of the lost energy to stored energy in a cyclic deformation. If the dynamic testing is done using small strain (within the linear viscoelastic region), the data obtained at higher and lower temperatures can be equated graphically with lower and higher frequencies, respectively, according to the principle of time-temperature equivalence.

The time-temperature superposition principle represents a powerful tool for evaluating dynamic loading data. Data obtained over a wide range of temperatures and a narrow

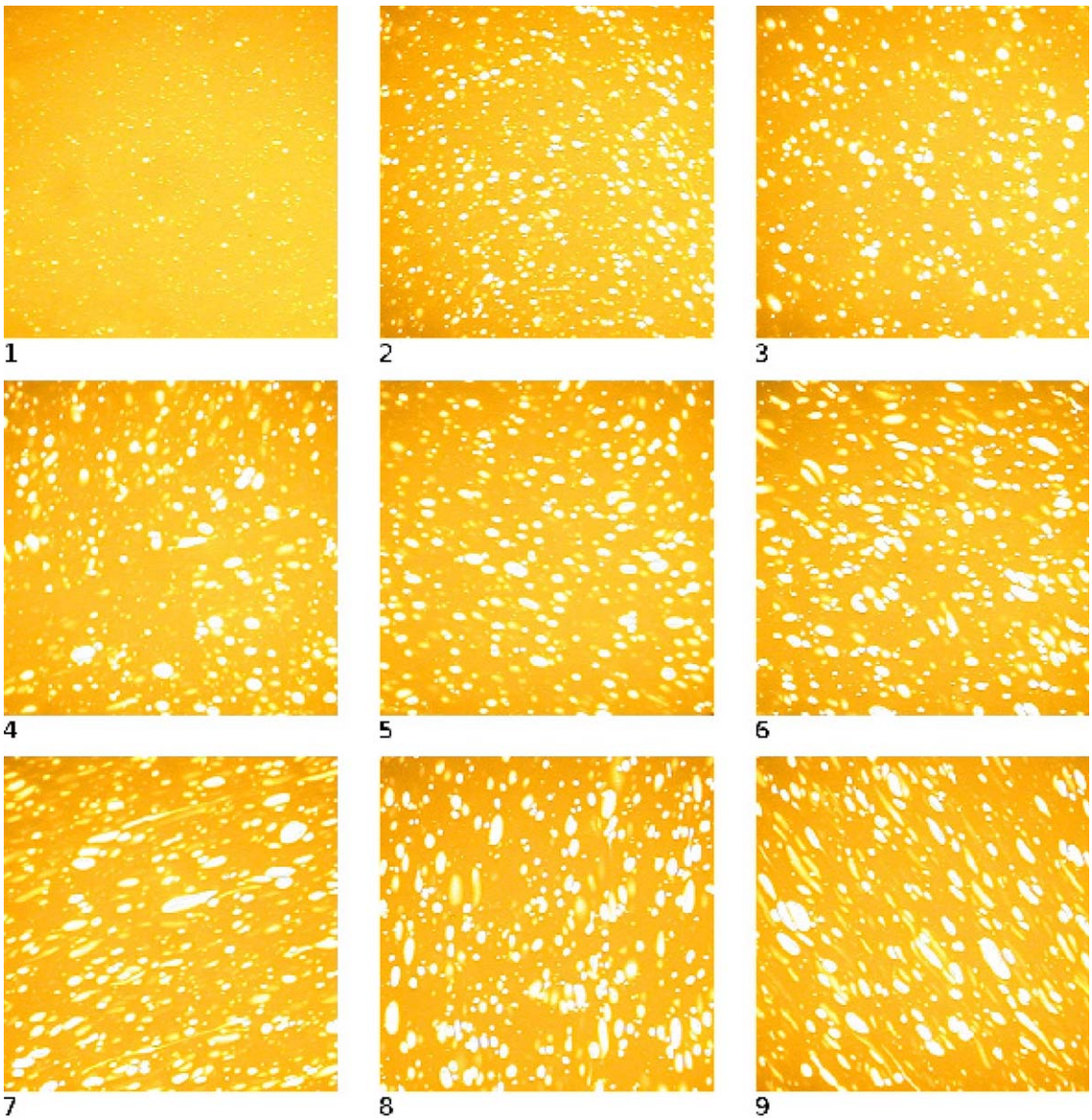

Figure 3. Evolution of microstructural properties for the PMB in the SR geometry.

Panel numbering indicates the number of hours elapsed from the start of the experiment. [Color figure can be viewed in the online issue, which is available at wileyonlinelibrary.com.]

range of frequencies can be shifted along the frequencies axis to form the Master Curve.

The polydispersity index (*PI*) is directly related to the ratio between the weight average aggregation number (Mw) and the number average aggregation number (Mn); it can be calculated from the value of complex modulus G^* when tan $\delta=1$ (named crossover modulus Gc) as $PI=10^5[\text{Pa}]/Gc$.

Rheological analyses were performed on the PMB samples obtained with axial symmetric and eccentric stirring by the Rushton impeller, **SR** and **ER**, respectively.

Results

Mixing assessment and microstructural properties

Results of experiments are next presented for the case of symmetric and eccentric stirring by the Rushton impeller, referred to as **SR** and **ER**, respectively, as well as for the case of the symmetric and eccentric disk impeller, next labeled **SD** and **ED**, respectively. The sequence of unprocessed images of the samples drawn at intervals of 1 h for the **SR** and **ER** protocol in shown in Figures 3, 4.

Several qualitative observations can be surmised from the comparison of these experiments. Primarily, one notes that after 1 h of stirring, almost no polymer phase reached the probing location of the sample in the **SR** protocol (panel "1" of Figure 3), whereas some degree of dispersion is already present in the **ER** stirring (panel "1" of Figure 4). Also, as time goes by, the area coverage of the polymer increases—although not strictly monotonically—for both protocols (see progressively numbered panels in the figures). In the **SR** protocol, the average clump size of the polymer phase does not appear to diminish sensibly over time, whereas this size is progressively reduced in the eccentric (**ER**) case, until no islands of the polymer phase are clearly visible after 7 h (panel "7" of Figure 4). Therefore, from the qualitative analysis of these experiments one gathers that both the dispersion

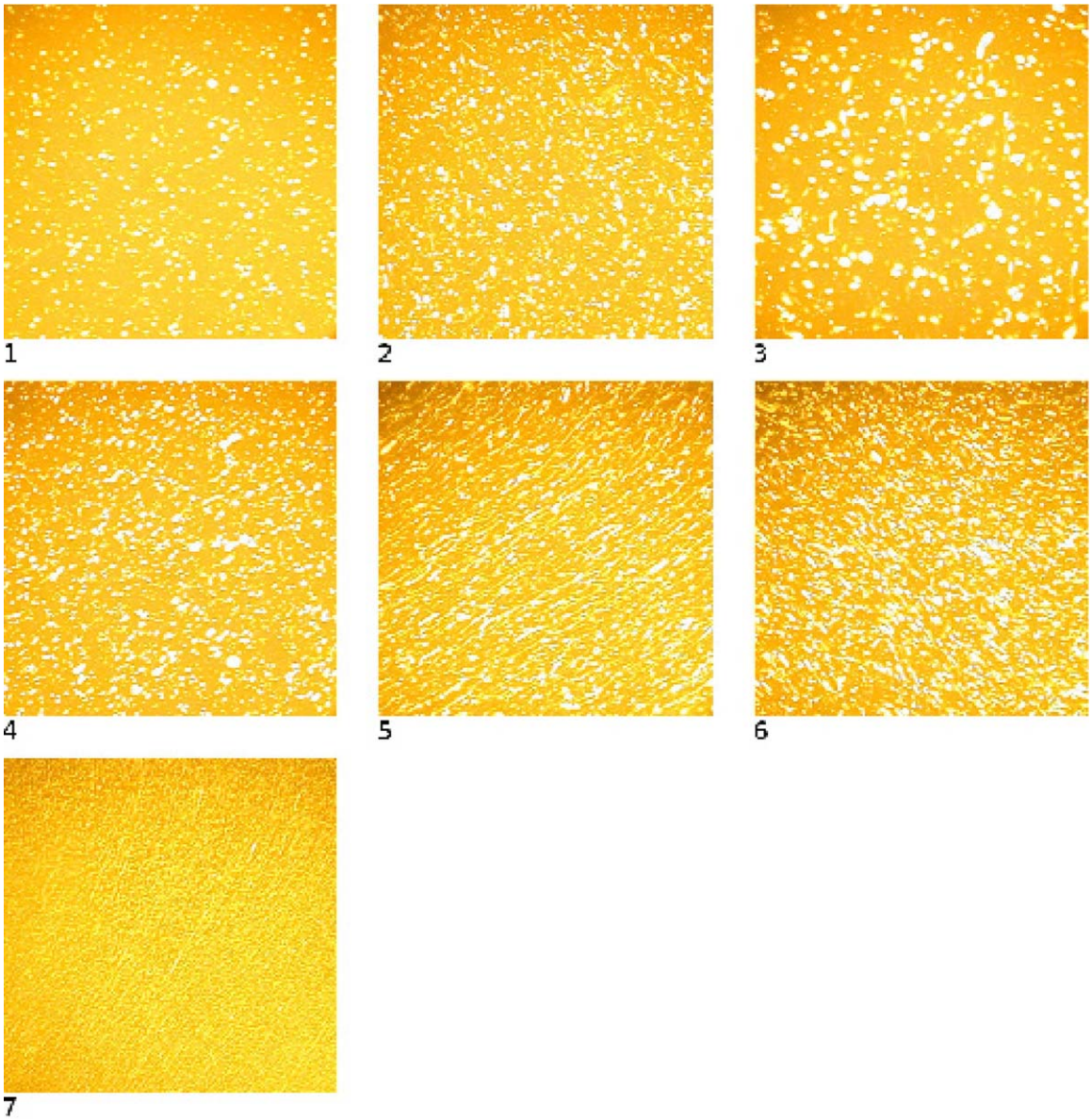

Figure 4. Evolution of microstructural properties for the PMB in the ER geometry.

Panel numbering indicates the number of hours elapsed from the start of the experiment. [Color figure can be viewed in the online issue, which is available at wileyonlinelibrary.com.]

process of the polymer phase throughout the vessel and the microstructural texture of the multiphase mixture are enhanced by the eccentric geometry **ER** with respect to the symmetric configuration.

Similar observations apply for the disk-stirred blending protocols, as illustrated by Figure 5, which shows the unprocessed photographs of PMB samples after 7 h of stirring for the symmetric (Figure 5a) and eccentric (Figure 5b) configurations.

Next, we try to put these observations on more quantitative grounds, starting from the dynamics of the dispersion process quantified by the surface coverage index *SI*. As discussed in the previous section, we use the theoretical framework developed for single-phase advecting-diffusing flows in closed systems for interpreting the dynamics of *SI* of the PMB. In this framework, one shows that for a scalar field, say $c(\mathbf{x},t)$ stirred by an advecting flow, at any point of the mixing domain the approach to the steady-state concentration c_{ss} can be characterized by an exponential backbone $c(\mathbf{x},t) \simeq c_{ss} + g(\mathbf{x})e^{-\Lambda t}$, where c_{ss} represent the total (average) concentration of the transported species in the entire vessel, and $\Lambda = 1/\theta_m$ is the inverse of a characteristic mixing time (see, e.g., Refs. 27 and 28 for the application of this approach to laminar and turbulent flows, respectively). It is worth observing that oscillations about this exponential decay may occur, depending on the structure of the flow. In the case object of the present study, at any time t, we take the concentration field $c(\mathbf{x},t)$ as the characteristic function $\chi(\mathbf{x})$, which assigns the value 0 if $\mathbf{x}$ belongs to the bituminous phase, and the value 1 whenever $\mathbf{x}$ belongs to the polymer-rich phase. Also, as functional structure for the time-dependence of the area-coverage fraction index, we use the simplified form

$$SI(t) = SI_{ss}\,(1 - e^{-\Lambda t}) \tag{3}$$

which can be obtained by the above relationship by setting $g(\mathbf{x}) = -c_{ss}$ (so that $SI(t=0)=0$), and regard the steady-state

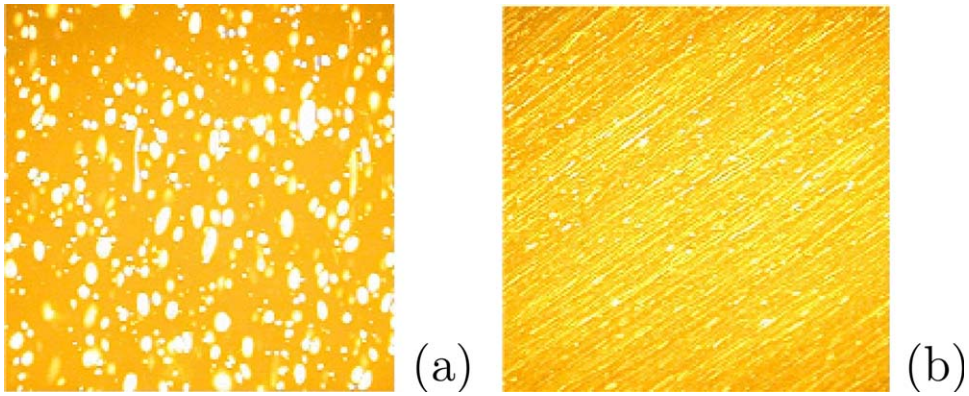

Figure 5. PMB microstructure for the (a) SD and (b) ED geometries after 7 h of stirring.

[Color figure can be viewed in the online issue, which is available at wileyonlinelibrary.com.]

area coverage fraction at the probe location, SI_{ss}, and the inverse mixing time, $\Lambda = 1/\theta_m$, as parameters to be estimated from best fit of experimentally measured values of *SI*. Because the exponential approach to steady-state conditions is expected to hold only at large times, in the estimate of SI_{ss} and Λ we disregard the early stage of the mixing process (i.e., data up to the first 3 h). Also, one observes that in our case the asymptotic value of *SI* depends only on the weight percentage of the polymer, and therefore should be considered constant in all of the experiments, regardless of the mixing strategy. Next, we use the **ER** protocol, which is expected to be the fastest in reaching steady-state conditions, to estimate the saturation value for *SI*. This value is then kept constant for all of the remaining protocols, for which Λ remains the only parameter to be estimated.

Figure 6 shows the experimental determination of the *SI* together with the best fit of the expression in Eq. 3 for the Rushton (Figure 6a), and disk (Figure 6b) geometries.

From the data depicted, one obtains $SI_{ss} \simeq 0.238$ for the saturation value of *SI*, and $\theta_m \simeq 88; 294; 158; 263$min for the mixing time in the **ER**, **SR**, **ED**, and **SD** geometries, respectively. For each impeller geometry, the eccentric configuration always performs better than the symmetric one. As expected, the comparison between different impeller geometries shows that similar values of mixing time can be obtained in the absence of impeller blades, thus suggesting that the mixing time is more influenced by the overall structure of the flow rather than the presence of temporal fluctuations of the velocity field.

It is worth remarking that while the mixing time and the dynamics of the surface coverage index *SI* provide valuable practical information about the operating conditions of the mixing process (e.g., it has been reported [29] that a low value of θ_m can prevent degradation of SBS when manufacturing PMB), no knowledge of the microstructural properties can be extracted from these data, in that samples characterized by the same *SI* index might possess altogether different morphologies of the multiphase mixture.

As discussed in the previous section, a global assessment for microstructural properties of PMB is afforded by the *MI*, which provides a modified version of the Mix-Norm, normalized to account for the local character of the probe sampling procedure. Figures 7a, b report the measures of this quantity for all of the protocols defined above. As regards the Rushton stirred protocols, one notes that very little influence of the stirrer placement (i.e., whether symmetric or eccentric) can be observed at the early stage of the mixing process (approximately extending over the first 3 h), whereas the final stage of stirring is characterized by an oscillatory behavior about a relatively large value of *MI* for the symmetric configuration, and an essentially monotonic decay for the eccentric geometry which yields the best performance among all of the geometries considered. The same observations apply to the case of disk stirred protocols, yet with the two curves departing from each other sooner than in the previous case. Observe that the **SD** protocol yields the worst performance, a result that is not altogether surprising in view of the regular (nonchaotic) kinematic structure that can be postulated for this geometry. We note, however, how the direct assessment of the kinematic character of the flow in molten PMBs represents a challenging task both

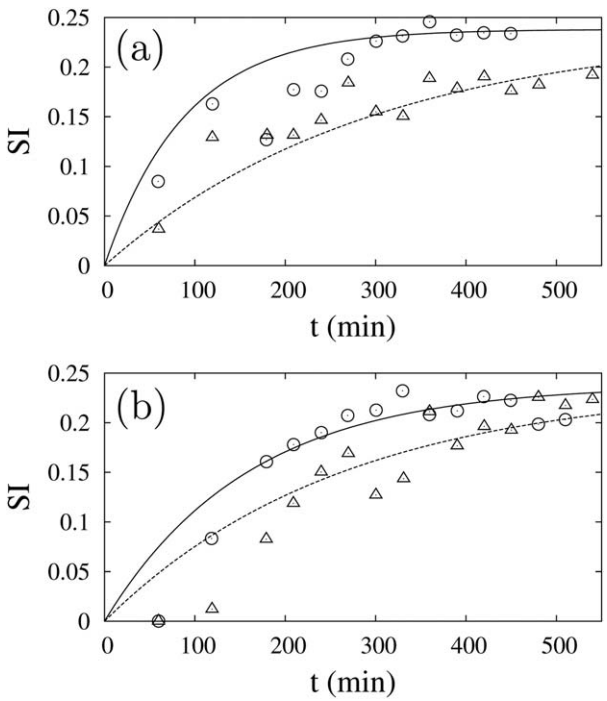

Figure 6. Experimental determination of *SI* for the Rushton (a) and disk (b) impeller.

Circles: eccentric geometry; triangles: symmetric geometry. Continuous and dashed curves represent the best fit to the data for eccentric and symmetric geometries, respectively (see main text for details).

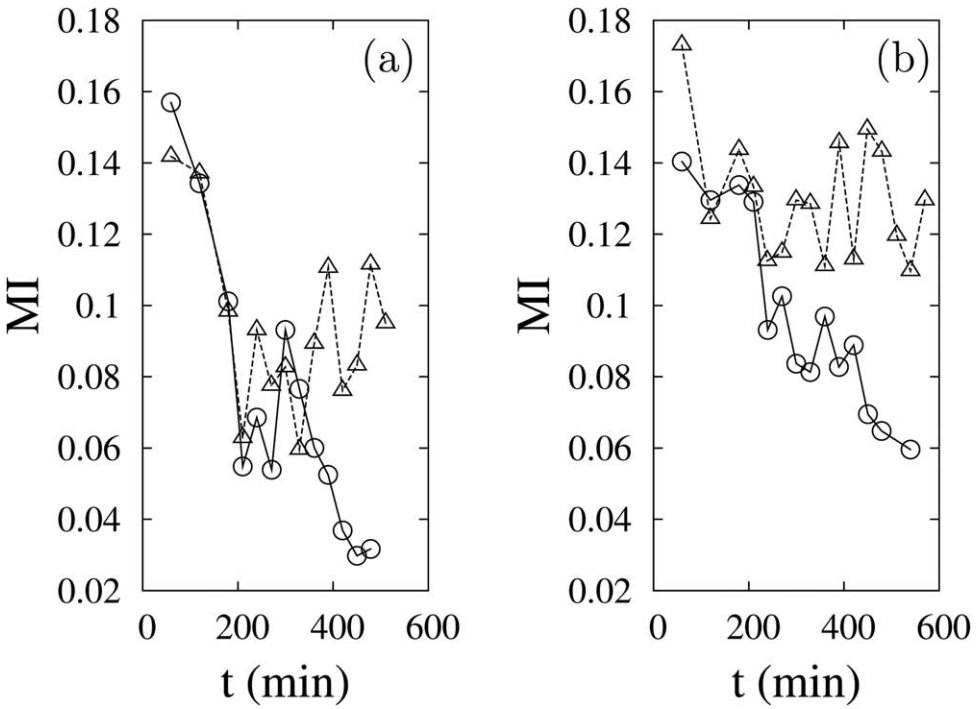

Figure 7. Panel (a): *MI* vs. time for the SR (triangles) and ER (circles) geometries.

Panel (b): *MI* vs. time for the SD (triangles) and ED (circles) geometries.

numerically—in view of the complex rheological behavior and multiphase nature of the molten mixture, and experimentally—because of the lack of optical transparency of the material.

Rheological properties

Rheological properties of the PMB samples obtained with axial symmetric and eccentric stirring by the Rushton impeller **SR** and **ER**, respectively, were compared to determine the effect of chaotic stirring on the quality of the products. In Table 2, the main rheological properties of **SR** and **ER** samples are reported. In single-phase mixture, the position of the crossover point (ω_c, G_c) of G' and G'' provides information on the molecular weight (Mw) and molecular weight distribution (MwD) of aggregates. Specifically, the crossover frequency ω_c is seen to be related to Mw, lowering with increasing Mw and vice versa) and almost independent of the MwD; on the contrary, the crossover point modulus (Gc) does not depend on Mw, while it increases with decreasing broadness of the MwD. In complex multiphase mixtures, such as the samples considered here, one can surmise that beyond the stand alone influence of the polymer phase (which we assume to possess the same features independently of the stirring process) the cross-over point can be strongly influenced by the interfacial adhesion that is associated with a given dispersion morphology of the polymer phase within the bitumen.[30] On the basis of these observations, the higher values of cross-over parameters ω_c and G_c displayed by the **ER** sample can be envisioned as a consequence of the reduced average clump size of the polymer phase and of its optimal dispersion, with a resulting decreasing value of *PI*.

A widely used graphical representation used to characterize the rheology of PMBs is the isotherm at 20°C of the complex modulus $G^*(\omega)$, that allows to predict the rheological behavior of this type of materials in their full-scale applications. The main curve of the complex modulus G^* against frequency is obtained according to the time-temperature equivalence, which is valid for a thermo-rheologically simple material. As illustrated in Figure 8a, the stirring protocol influences the complex modulus G^* in the whole range of temperatures scanned. Specifically, the complex modulus for sample **ER** is higher than that of **SR** sample in the whole range of frequencies, corresponding to an increment of both the viscous and elastic components, G'' and G', respectively. Also, the increasing of complex modulus observed for the **ER** sample as compared to the **SR** one is greater at high frequencies (low temperatures). The influence of the stirring protocol on the viscous and elastic components was quantified analyzing the difference between the values of G'' and G' obtained for **SR** and **ER** samples, next labeled $\Delta G''_{ER-SR}$ and $\Delta G'_{ER-SR}$, respectively, which are reported in Figure 8b. As can be observed, the eccentric stirring confers to sample **ER** higher values of G' and G'' in the entire range of frequencies. From all of the data shown, one concludes that the effect of the eccentric stirring protocol on both the viscous and the elastic components is such as to confer better rheological performance for PMB in the range of temperatures scanned, owing to the greater contribution of the elastic

Table 2. Rheological Properties of SR and ER Samples.

Sample	ω_c(rad/s)	G_c(Pa)	PI
SR	125.89	1.20×10^7	0.0083
ER	191.95	2.98×10^7	0.0035

All data are obtained from master curves at the reference temperature $T = 20$°C.

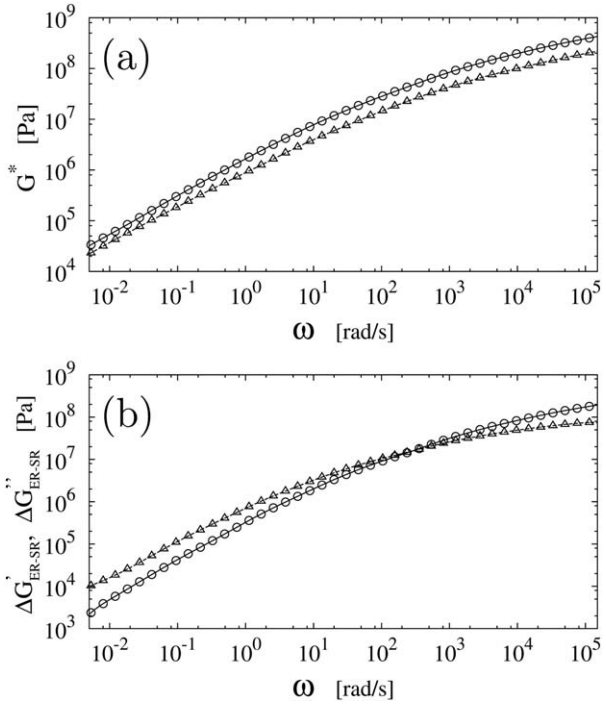

Figure 8. Panel (a): Complex modulus at 20°C for the ER (circles) and SR (triangles) PMB samples.

Panel (b): Increase of elastic (circles) and viscous (triangles) components of the complex modulus due to chaotic mixing.

modulus at low temperatures, and of the viscous modulus at relatively high temperatures.

Conclusions

It is well established that key physical–chemical properties of bitumen and of PMB may depend sensitively on equipment geometry and operating conditions during the emulsion stage of the production process. Best quality product is typically obtained when using high-shear blenders, such as the rotor-stator mixer, which, in turn, are characterized by large energy dissipation and severe mechanical constraints. In this article, we approach the problem along a different view angle, trying to single out the basic mechanisms that are ultimately responsible for favorable properties of PMBs, which demand a uniform and finely interdispersed structure of the multiphase mixture. Based on previous results focusing either on single-phase systems or on low-viscosity multiphase mixtures, we devise stirring protocols that are expected to yield chaotic kinematics of fluid elements. We define objective measures for the homogenization dynamics (quantified by the mixing time characterizing the saturation of the surface-coverage index *SI*) as well as for the microstructural properties of the mixture, for which we propose a modified version of the Mix-Norm as a global measure. By comparing different laminar stirring protocols taking place in a cylindrical vessel, we find that both the dispersion dynamics and the microstructural properties of the mixture are enhanced in those geometries that are known to yield chaotic kinematic when applied to fluids with simple rheological behavior (e.g., Newtonian). Results of the rheological characterization of samples drawn in different stirring conditions are consistent with the measures assessing the microstructural quality of the two-phase mixture. By reason of these qualitative and quantitative results, it is sensible to assume the ultimate mechanism improving both the process time and the morphological quality of the product mixture in SBS-modified bitumen is to be ascribed to chaotic stirring. This observation raises the question whether a well-designed mixing equipment operating in the laminar regime can yield a product of comparable quality with respect to those obtained through standard manufacturing processes, while being less demanding both in terms of equipment investment and energy consumption.

Literature Cited

1. Whiteoak D. *The Shell Bitumen Handbook*. Riversdell House, Surrey, UK: Shell Bitumen UK, 1990.
2. Yen TF. Colloidal aspect of a macrostructure of petroleum asphalt. *Fuel Sci Technol Int*. 1992;10(4–6):723–733.
3. Murgich J, Jesus Rodriguez M, Aray Y. Molecular recognition and molecular mechanics of micelles of some model asphaltenes and resins. *Energy Fuels*. 1996;10(1):68–76.
4. Sirota E. Physical structure of asphaltenes. *Energy Fuels*. 2005; 19(4):1290–1296.
5. Loeber L, Durand A, Mueller G, Morel J. New investigations on the mechanism of polymer-bitumen interaction and their practical application for binder formulation. In: Eurasphalt and Eurobitume Congress; E & E.5.115. Strasbourg: International Institute of Informatics and Systemics, 1996.
6. Hanyu A, Kasahara A, Saito K. Effect of the morphology of SBS modified asphalt on mechanical properties of binder and mixture. *J East Asia Soc Transp Studies*. 2005;6:1153–1167.
7. Sengoz B, Topal A, Isikyakar G. Morphology and image analysis of polymer modified bitumens. *Constr Build Mater*. 2009;23(5):1986–1992.
8. Bouldin M, Collins J, Berker A. Rheology and microstructure of polymer/asphalt blends. *Rubber Chem Technol*. 1991;64(4):577–600.
9. May J, Winkley T. Heating, mixing and storing modified asphalt. Technical Paper T-133, Heatec Inc (Austec Indistries), 1999.
10. Gingras JP, Tanguy P, Mariotti S, Chaverot P. Effect of process parameters on bitumen emulsions. Chem Eng Process. *Process Intensif*. 2005;44(9):979–986.
11. Zhang J, Xu S, Li W. High shear mixers: a review of typical applications and studies on power draw, flow pattern, energy dissipation and transfer properties. *Chem Eng Process. Process Intensif*. 2012; 57–58:25–41.
12. Sundararajan P, Stroock A. Transport phenomena in chaotic laminar flows. *Annu Rev Chem Biomol Eng*. 2012;3:473–496.
13. Metcalfe G, Speetjens M, Lester D, Clercx H. Beyond passive. Chaotic transport in stirred fluids. *Adv Appl Mech*. 2012;45:109–188.
14. Aref H. Stirring by chaotic advection. *J Fluid Mech*. 1984;143:1–21.
15. Cerbelli S, Alvarez M, Muzzio F. Prediction and quantification of micromixing intensities in laminar flows. *AIChE J*. 2002;48(4):686–700.
16. Alvarez M, Zalc J, Shinbrot T, Arratia P, Muzzio F. Mechanisms of mixing and creation of structure in laminar stirred tanks. *AIChE J*. 2002;48(10):2135–2148.
17. Alvarez M, Arratia P, Muzzio F. Laminar mixing in eccentric stirred tank systems. *Can J Chem Eng*. 2002;80(4):546–557.
18. Irene Sanchez Cervantes M, Lacombe J, Muzzio F, Alvarez M. Novel bioreactor design for the culture of suspended mammalian cells. Part I: Mixing characterization. *Chem Eng Sci*. 2006;61(24): 8075–8084.
19. Cabaret F, Fradette L, Tanguy P. Effect of shaft eccentricity on the laminar mixing performance of a radial impeller. *Can J Chem Eng*. 2008;86(6):971–977.
20. Bulnes-Abundis D, Carrillo-Cocom L, Araiz-Hernandez D, Garcia-Ulloa A, Granados-Pastor M, Sanchez-Arreola P, Murugappan G, Alvarez M. A simple eccentric stirred tank mini-bioreactor: mixing characterization and mammalian cell culture experiments. *Biotechnol Bioeng*. 2013;110(4):1106–1118.
21. Lester D, Rudman M, Metcalfe G. Low Reynolds number scalar transport enhancement in viscous and non-Newtonian fluids. *Int J Heat Mass Transf*. 2009;52(3–4):655–664.
22. Ottino J. Unity and diversity in mixing: Stretching, diffusion, breakup, and aggregation in chaotic flows. *Phys Fluids A*. 1991;3(5): 1417–1430.

23. Habchi C, Lemenand T, Della Valle D, Peerhossaini H. Liquid/liquid dispersion in a chaotic advection flow. *Int J Multiphase Flow*. 2009; 35(6):485–497.
24. Mathew G, Mezic I, Petzold L. A multiscale measure for mixing. *Phys D*. 2005;211(1–2):23–46.
25. Bulnes-Abundis D, Alvarez M. The simplest stirred tank for laminar mixing: mixing in a vessel agitated by an off-centered angled disc. *AIChE J*. 2013;59(8):3092–3108.
26. Hartmann H, Derksen J, Van Den Akker H. Mixing times in a turbulent stirred tank by means of LES. *AIChE J*. 2006;52(11):3696–3706.
27. Cerbelli S, Adrover A, Creta F, Giona M. Foundations of laminar chaotic mixing and spectral theory of linear operators. *Chem Eng Sci*. 2006;61(9):2754–2761.
28. Giona M, Paglianti A, Cerbelli S, Pintus S, Adrover A. Tracer dispersion in stirred tank reactors: asymptotic properties and mixing characterization. *Can J Chem Eng*. 2002;80(4):580–590.
29. Larsen D, Alessandrini J, Bosch A, Cortizo M. Microstructural and rheological characteristics of SBS-asphalt blends during their manufacturing. *Constr Build Mater*. 2009;23(8):2769–2774.
30. Gonzlez O, Pena J, Munoz M, Santamaria A, Perez-Lepe A, Martinez-Boza F, Gallegos C. Rheological techniques as a tool to analyze polymer-bitumen interactions: bitumen modified with polyethylene and polyethylene-based blends. *Energy Fuels*. 2002;16(5): 1256–1263.

Manuscript received Oct. 31, 2013, and revision received Dec. 22, 2013.